Flow over riblet curved surfaces



2011 J. Phys.: Conf. Ser. 318 022035

(http://iopscience.iop.org/1742-6596/318/2/022035)

# Flow over riblet curved surfaces

**J. B. R. Loureiro & A. P. Silva Freire**

Mechanical Engineering Program, Federal University of Rio de Janeiro (COPPE/UFRJ), C.P. 68503, 21.941-972, Rio de Janeiro, RJ, Brazil.

E-mail: atila@mecanica.ufrj.br

**Abstract.** The present work studies the mechanics of turbulent drag reduction over curved surfaces by riblets. The effects of surface modification on flow separation over steep and smooth curved surfaces are investigated. Four types of two-dimensional surfaces are studied based on the morphometric parameters that describe the body of a blue whale. Local measurements of mean velocity and turbulence profiles are obtained through laser Doppler anemometry (LDA) and particle image velocimetry (PIV).

## 1. Introduction

The forces of resistance to the motion of a body are in most applications dominated by the viscous component. According to Frohnapfel et al. (2007) the viscous contribution to the total drag accounts to 50% on civil aviation, 90% on naval engineering and almost 100% on pipe flows.

In a near wall flow, most of the turbulent activity occurs at a very small scale, typically of the order of a few wall unit lengths, $\nu/u_*$, where $\nu$ denotes the kinematic viscosity of the fluid and $u_*$ the friction velocity. In fact, 80% of the total production of turbulence occurs near the wall, in the first 5% of the boundary layer (Lu & Willmarth 1973). In this region, some structural organization can be observed, consisting of elongated, counter-rotating, streamwise vortices with diameters of approximately 40 wall units. These vortices appear to be sufficiently regular with an average spanwise wavelength of 80 to 100 wall units.

The existence of a well defined near wall structure dominated by low speed streaks suggests that passive and active methods could be used to control the properties of a boundary layer and, in special, to reduce viscous drag (Gad-el-Hak & Bandyopadhyay 1994). To serve this purpose, several techniques have been studied in literature: polymer addition, compliant surfaces, wall transpiration, riblets and vortice generators (Gad-el-Hak 2000).

The objective of the present work is to investigate the mechanics of turbulent drag reduction by streamwise aligned micro-grooved striations, also referred to as riblets, for flow over curved surfaces. This is a problem that is rarely addressed in literature. Most works focus their attention on flow over flat surfaces (Karniadakis & Choi 2003). Here, the effects of surface modification on flow separation over steep riblet surfaces are investigated. Four different surfaces are tested: (i) a symmetric smooth surface, (ii) an asymmetric smooth surface, (iii) a symmetric riblet surface and (iv) an asymmetric riblet surface.

A discussion on the particular type of surfaces that were studied here is presented next. We anticipate that steep symmetric surfaces were considered so that flow separation could be observed on their lee. Asymmetric surfaces were also designed with a slow deceleration of

the downflow so that flow separation was prevented. These two types of surface – symmetric and asymmetric – allow the assessment of drag reduction effects through the interplay between shape geometry and riblet walls. Local measurements of mean velocity and turbulence profiles are obtained through laser Doppler anemometry (LDA) and particle image velocimetry (PIV).

## 2. Experiments

### *2.1. Geometry of surfaces*

In Nature, the optimization of energy expenditure by aquatic mammals has benefited from evolutionary convergence. In addition to adaptations aimed at improving thrust, drag reduction plays an important role on energy savings (Fish & Lauder 2006). Drag minimization is achieved by streamlining the shape of the body and appendages. However, the morphology of body, fluke and flipper vary greatly among species (Fish 1993). The morphological characteristics of the blue whale (*Balaenoptera musculus*) suggests that drag reduction may be obtained by riblets.

The two types of two-dimensional surfaces studied in the present work were inspired on the morphometric parameters that describe the body of a blue whale (Becky et al. 2006). A symmetric steep curved surface was constructed from a reflection of the aft body shape of a blue whale around its apex, the point of maximum body thickness. The asymmetric smooth curved surfaces follow the geometry shown in red in Figure 1. The latter configuration is highly streamlined, thus preventing flow separation.

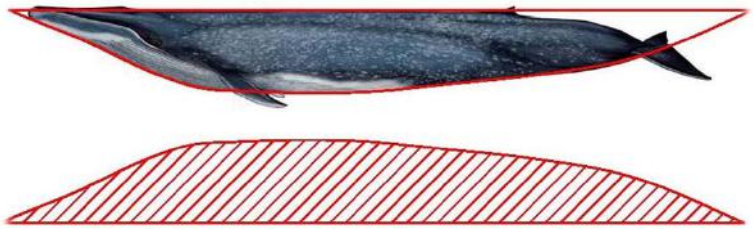

**Figure 1.** Morphometric features of a blue whale.

Figure 2 shows the general forms of both surfaces: symmetric and asymmetric. The models were made in fiber-glass. The asymmetric model is 450 mm long whereas the symmetric one is 350 mm long. Both geometries are 500 mm wide and 50 mm thick. The cross-section of the riblets is given also shown in Figure 2. A mechanical pencil is used to illustrate the scale of the models.

### *2.2. Wind tunnel and instrumentation*

The experiments were carried out in the low-turbulence wind tunnel of the Fluid Mechanics Laboratory of the Brazilian National Institute of Standards. The tunnel is an open circuit tunnel with a test section of 0.5 x 0.5 x 8 m.

Mean velocity and turbulence statistic data were obtained with a two-component laser Doppler anemometer (LDA) and a two-dimensional particle image velocimeter (PIV).

The two-component TSI laser-Doppler anemometry system used a 400 mW Ar-ion tube laser and was operated in the forward-scatter mode to measure mean and fluctuating velocity fields. A Bragg cell unit was used to introduce a digitally-controlled electronic shift in order to resolve the direction of the flow field and give correct measurements of near-zero mean velocities. A

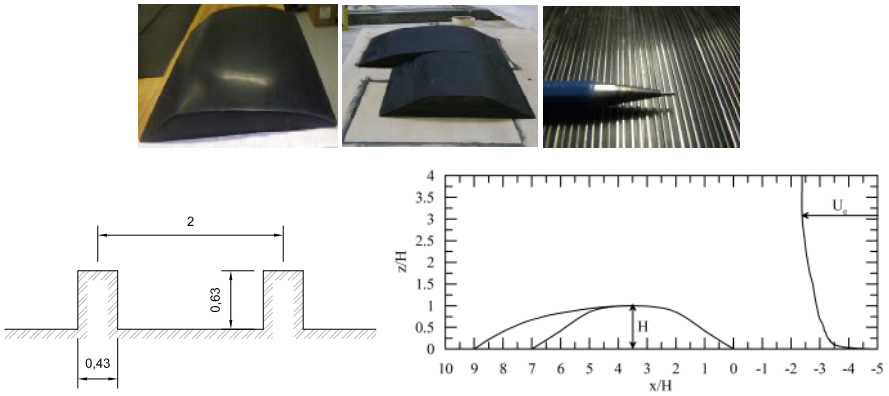


**Figure 2.** Model shapes, geometry of riblets and coordinate system. Dimensions are in mm.

series of LDA biases were avoided by adjusting the strictest parameters on the data processor and software.

In the experiments, the total number of samples for every point of velocity measurement was adjusted to ensure statistical independence between consecutive measurements as well as to furnish an interval of confidence of 95%. The overall uncertainty is expressed in percentages of the free stream velocity, $U_e$ (for the mean velocities) and the square of the friction velocity, $(u_*^2)$ (for the Reynolds stress components). Typical uncertainties associated with the mean velocity data – $U$ – are below $0.2\%U_e$. Regarding the second order moments, uncertainties were estimated to be $2.3\%u_*^2$.

The PIV measurements were performed with a two-dimensional Dantec Dynamics system. The light source was furnished by a double pulsed Nd:YAG laser that produced short duration (4 ns) high energy (135 mJ) pulses of green light (532 nm). The reflected light by the particles was recorded at 7.5 Hz by a CCD camera with 2048 x 2048 pixels and 10-bit resolution. The camera was fitted with a Nikkor 60 mm f/2.8D lens. A total of 3,000 image pairs were acquired for each calculation of mean velocity and turbulent statistics of the flow. Image calibration was made by taking pictures of a reference target specially designed for the present purpose.

For all the measurements, computational conditions for the velocity vectors were fixed. Adaptive correlation (Dynamic Studio Software) has been processed using one refinement step, no overlap and initial and final interrogation areas of 64x64 and 32x32 pixels, respectively. This procedure furnished a final map of the flow with 127x127 vectors. The pixel resolution is 6.45x6.45 $\mu$m. Particle image treatment using high accuracy subpixel refinement allowed bias and random error reduction. A widely accepted estimation of the absolute displacement error using these algorithms is 0.05 pixels. Different thresholds including signal-to-noise ratio and local neighborhood validation were used as post-processing steps.

For both the LDA and PIV techniques, seeding was provided by a Laskin nozzle.

## 3. Results

The overall drag performance of all four surfaces is presented in Figure 3 for Reynolds number ($Re$) up to 66,260 ($Re = U_eH/\nu$, $H$ = model height, $U_e$ = external flow velocity). For $R_e <$ 33,150, the riblet surfaces (open symbols) always perform better than the smooth surfaces, i.e., they exhibit a local smaller value of $C_d$ ($= \Delta P/(0.5\ \rho U^2)$, where $\Delta P$ is taken before and after the curved surfaces). The highest reductions in $C_d$ are observed on the left end of Figure 3, for $R_e$ = 8,900; they are of the order of 10%. For $R_e$ higher than approximately 33,150 the reduction in $C_d$ still persists for the asymmetric geometry but is much less pronounced. For the

symmetric geometry, the trend seems to be reversed. For $R_e > 33{,}150$ a small increase in $C_d$ is noted for the riblet surface.

In general, in the whole range of Reynolds number the riblet surfaces perform better than the smooth surfaces. For the higher $Re$'s, a higher $C_d$ for the symmetric riblet surface (as compared to the smooth surface) has been consistently observed.

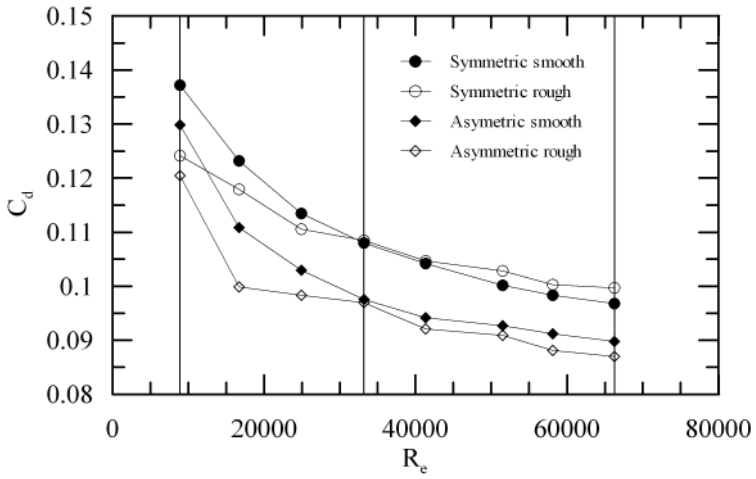


**Figure 3.** Drag coefficient for the four tested surfaces. The three vertical lines correspond to $R_e$ = 8,900, 33,150 and 66,260.

To better understand the results of Figure 3, let us consider the streamlines of all four surfaces for $R_e$ = 8,900, 33,150 and 66,260.

The forms of the lines of motion for the symmetric geometries – smooth and riblet – are shown in Figure 4. The extent of separated flow at $R_e$ = 8,900 for both surfaces is about the same; the position of the separation and reattachment points, in particular, are located at the same positions. For $R_e$ higher than 33,150, the separation and reattachment points for flow over the riblet surfaces move upstream and downstream respectively, whereas for the smooth surface they remain almost unaltered. The increase in extent of the reverse flow region for the riblet surface can be further appreciated in Figure 5. The distribution of turbulent kinetic energy ($\kappa$) in Figures 5a, 5c and 5e is about the same. Figures 5b, 5d and 5f, on the other hand display a completely different behaviour. Skote & Hennigson (2002) have confirmed through direct numerical simulation that the peak in turbulent kinetic energy is located outside of a recirculation region. In general, in regions of reverse flow, turbulence profiles are characterized by an elevated maximum, whose distance to the wall increases with increasing distance from a hill (Loureiro et al. 2007). In Figures 5b, 5d and 5f regions with high $\kappa$ (green, light blue) are well dislocated from the wall, indicating the presence of a large recirculation bubble. The large regions of separated flow induce an increase in $C_d$ for the riblet surfaces for $R_e > 33{,}150$.

The different flows over the two asymmetric surfaces – smooth and riblet – are shown in Figure 6. Over the smooth surface, the flow always remains attached (Figures 6a, 6c, 6e). Over the riblet surface, for $R_e$ = 33,150 and 66,260, small regions of separated flow are identified at the trailing edge (Figures 6d, 6f). These regions are further noted in Figure 7, which illustrates how the peaks of $\kappa$ are pushed away from the wall (Figures 7d, 7f). Orlandi et al. (2006) have reported that for a riblet wall the increase in $\kappa$ is restricted to a thin layer close to the plane of the roughness crests. Here, for $R_e$ = 8,900 (attached flows) the near wall levels of $\kappa$ are reduced compared with the smooth surface values (Figures 7a, 7b).

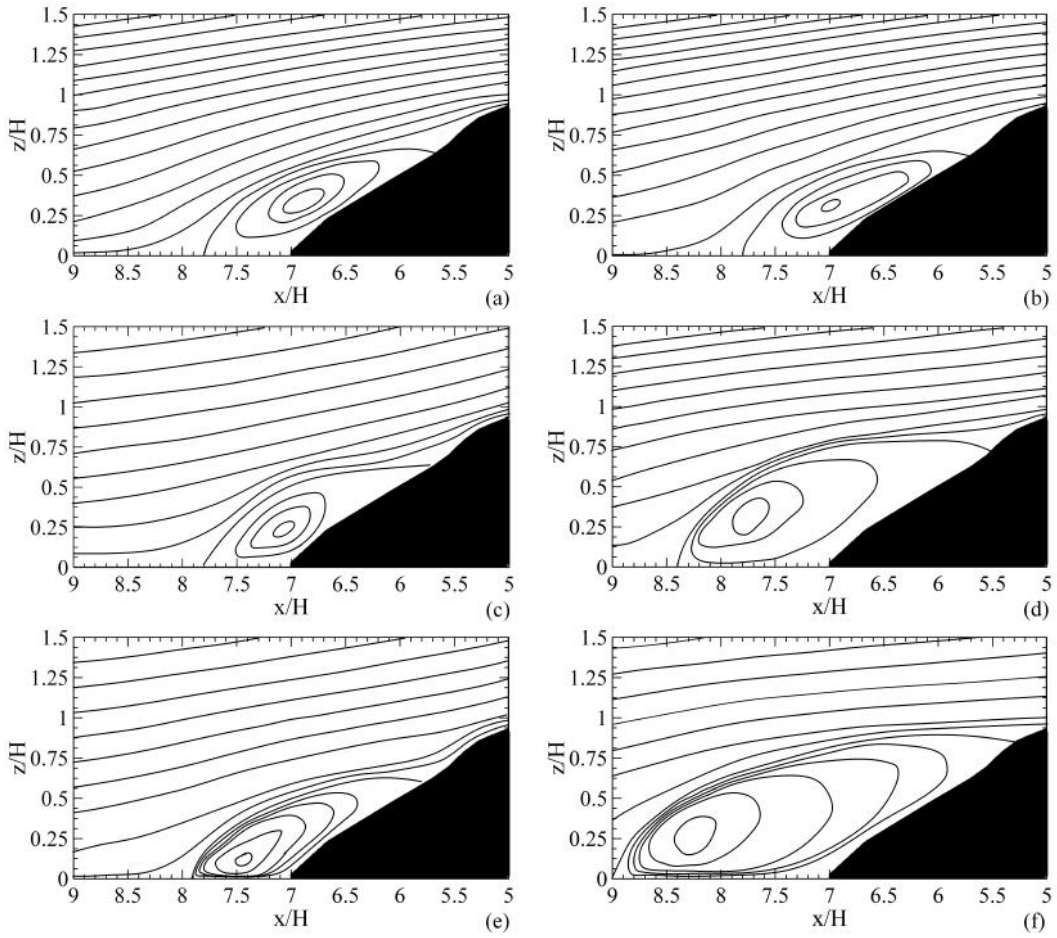


**Figure 4.** Streamlines of the flow over the two symmetric models. Left column, smooth surface: (a) $R_e$ = 8,900, (c) $R_e$ = 33,150, (e) $R_e$ = 66,260. Right column, riblet surface: (b) $R_e$ = 8,900, (d) $R_e$ = 33,150, (f) $R_e$ = 66,260.

The overall effect of the riblets for the asymmetric surface is to reduce drag. Even with the existence of a small separation region for $R_e$ higher than 33,150, drag is always reduced for the asymmetric riblet surface.

The position of the separation and reattachment points for all studied situations is consolidated in Table 1. The length of the separation bubble is also shown.

The PIV measurements were complemented by some selected LDA measured profiles at $R_e$ = 8,900. Four positions were selected (see inset in Figure 8a), two at the top of the surface, one at the separation point and one in the reverse region.

The mean velocity profiles are shown in Figure 8. The region of reverse flow (negative velocities) for the symmetric profile is clearly identified (Figure 8a). The velocity speed-up at the apex of the surfaces is observed at $x/H = 3.5$ and 4.1. The strong external flow deceleration is apparent at positions $x/H = 5.7$ and 6.5 (Figure 8a).

The longitudinal turbulent shear stress is shown in Figure 9. The high shear rates in the mixing region between the separation bubble and the external flow increase four times from its undisturbed values (Fig. 9a, $x/H = 6.5$). The position of the peak in shear stress moves away from the wall.

Figure 9b shows that much lower turbulence levels are observed for the asymmetric curved

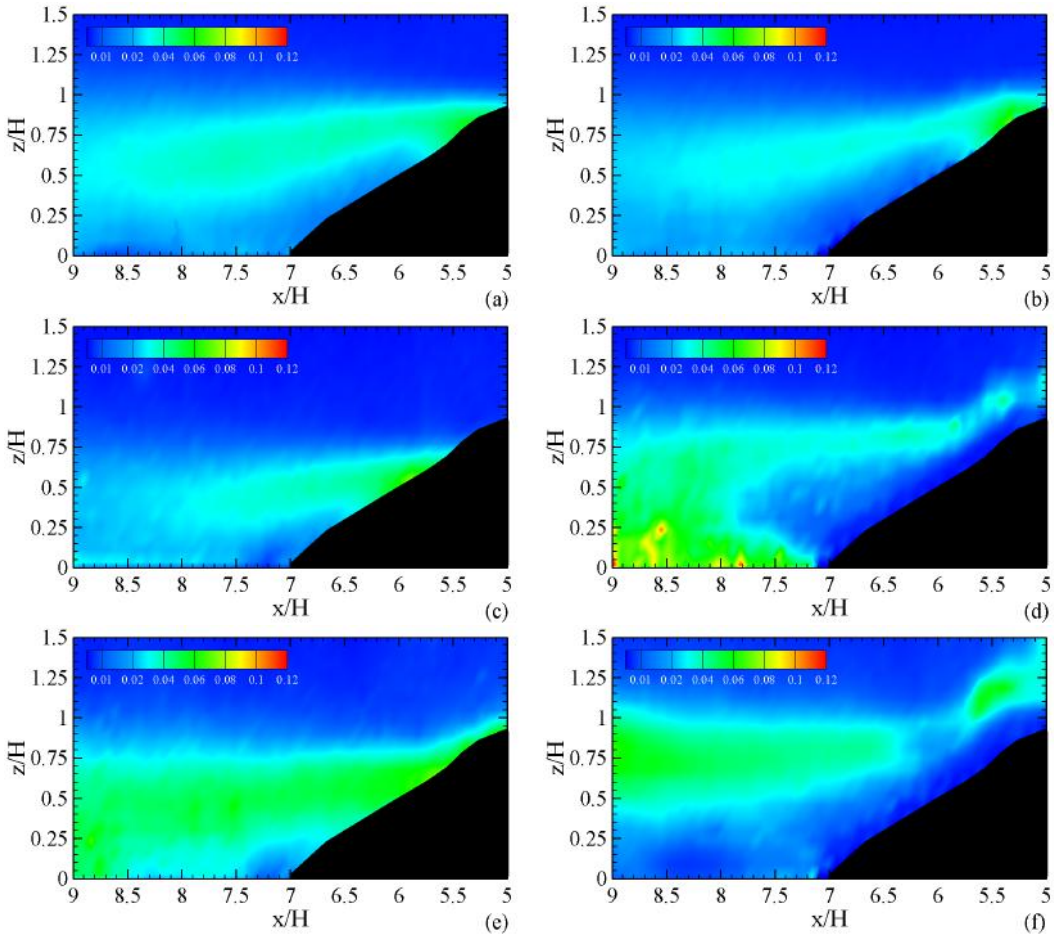


**Figure 5.** Nondimensional turbulent kinetic energy ($\kappa/U_e^2$) for the flow over the two symmetric models. Left column, smooth surface: (a) $R_e$ = 8,900, (c) $R_e$ = 33,150, (e) $R_e$ = 66,260. Right column, riblet surface: (b) $R_e$ = 8,900, (d) $R_e$ = 33,150, (f) $R_e$ = 66,260.

surface, as compared to the symmetric surface. This is explained by the slow flow deceleration that occurs over the asymmetric surface, which leads to less turbulence production due to the lower mean velocity gradients.

An important aspect for the successful use of riblets seems to be their ability to isolate the wall from the turbulence by maintaining laminar flow in the valleys. An assessment of the amount of turbulence that penetrates into the riblet cavities can be given by the third-order moments ($S_u$). Unfortunately, our LDA results only cover the smooth surface cases. These are reported next.

Flow regions where $S_u$ is positive are associated with acceleration dominated velocity fluctuations resulting from the arrival of external high-speed fluid (sweep events) (Gad-el-Hak & Bandyopadhyay 1994).

The region of separated flow expands the region of violent positive fluctuations (Figure 10a). After the dip to negative values, no values of $S_u$ close to those of a Gaussian distribution ($S_u$ = 0) are recorded. At position $x/H$ = 6.5, negative values of $S_u$ very close to the wall are observed. Over the asymmetric surface, the canonical behaviour of $S_u$ for flow in boundary layers is observed (Figure 10b).

The flatness results presented in Figure 11 show a very high intermittent motion near the

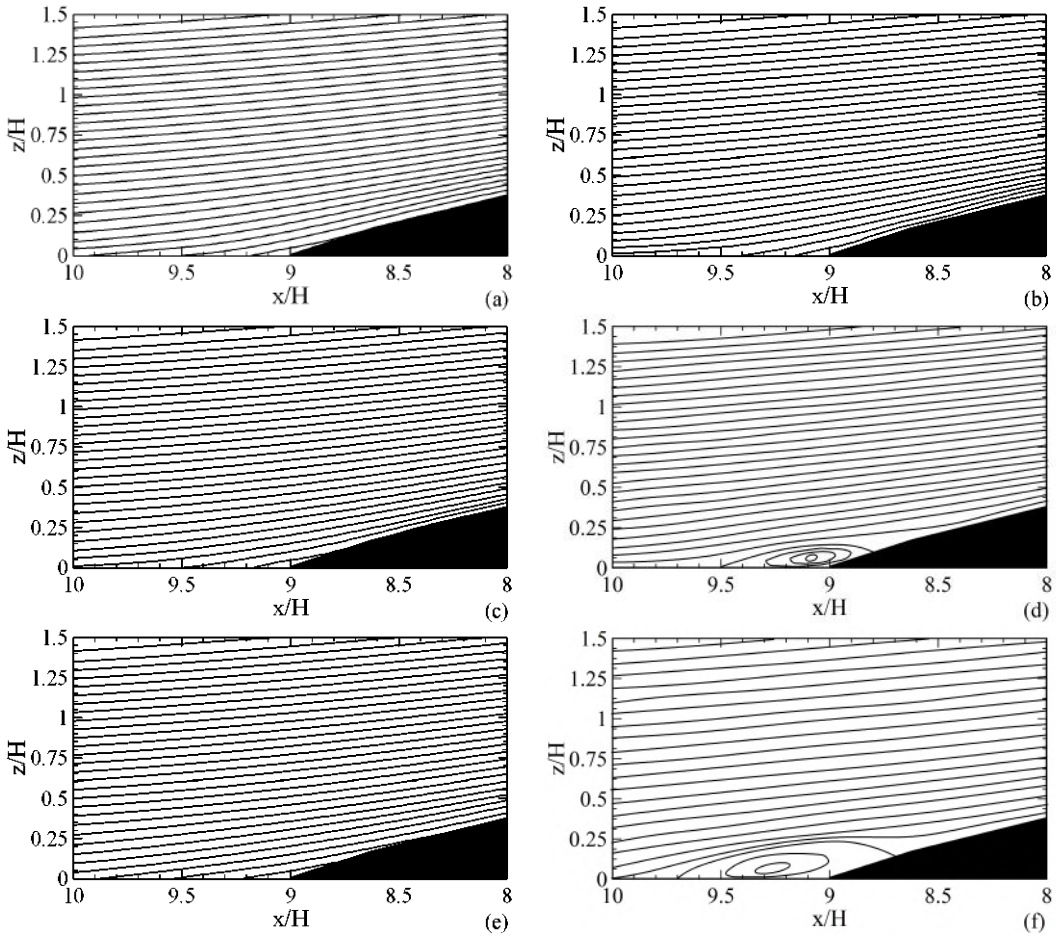


**Figure 6.** Streamlines of the flow over the two asymmetric models. Left column, smooth surface: (a) $R_e$ = 8,900, (c) $R_e$ = 33,150, (e) $R_e$ = 66,260. Right column, riblet surface: (b) $R_e$ = 8,900, (d) $R_e$ = 33,150, (f) $R_e$ = 66,260.

wall and in the outer layer. The region of reverse flow promotes highly intermittent motions that persist up to $z/H \approx 0.3$ (peak value of 10)(Figure 11a).

## 4. Final remarks

The present work shows that riblet surfaces can be used to reduce drag in flows over curved surfaces with flow separation. The results show that for the whole Reynolds number domain, the asymmetric riblet surface performs better than all the other surfaces.

Further experiments are currently under way so that a complete PIV and LDA characterization of all four surfaces can be achieved. In addition, new types of surfaces will be tested.

## Acknowledgments

Acknowledgments JBRL benefited from a CNPq Research Fellowship (Grant No 301172/2010-2). JBRL is also thankful to the Brazilian National Research Council (CNPq) for the financial support to this research through Grant 475759/2009-5. APSF is grateful to the

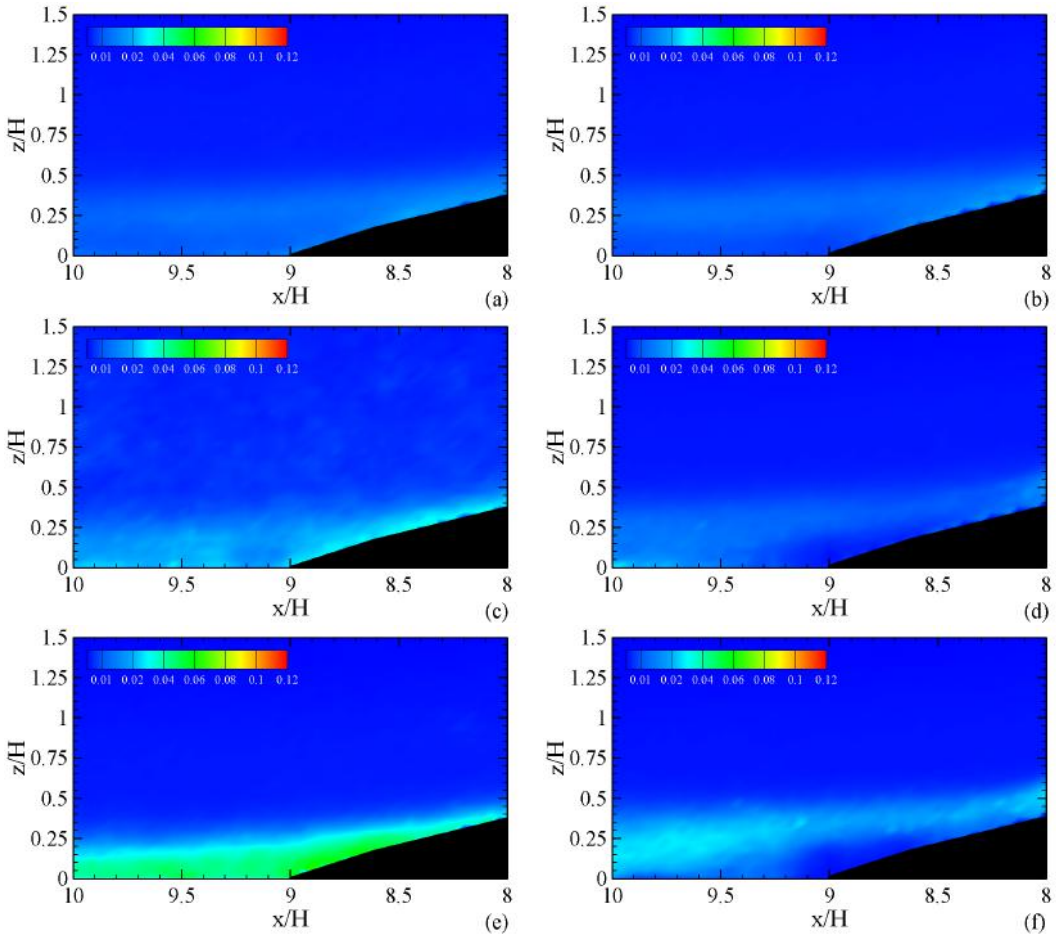


**Figure 7.** Nondimensional turbulent kinetic energy ($\kappa/U_e^2$) for the flow over the two asymmetric models. Left column, smooth surface: (a) $R_e$ = 8,900, (c) $R_e$ = 33,150, (e) $R_e$ = 66,260. Right column, riblet surface: (b) $R_e$ = 8,900, (d) $R_e$ = 33,150, (f) $R_e$ = 66,260.

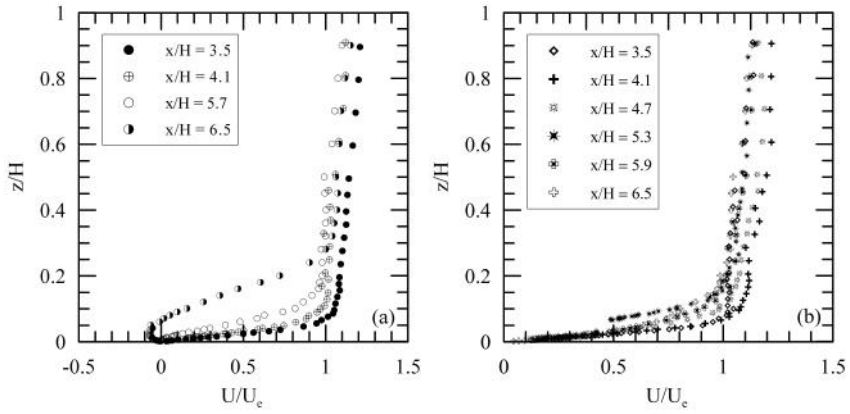


**Figure 8.** Mean velocity profiles: (a) symmetric surface, (b) asymmetric surface.

**Table 1.** Length of separated flow ($L/H$) according to the PIV experiments.

| Model | Reynolds number | Separation point ($x/H$) | Reattachment point ($x/H$) | Length $L/H$ |
|---|---|---|---|---|
| Symmetric, smooth | 8,900 | 5.7 | 7.8 | 2.1 |
| Symmetric, riblets | 8,900 | 5.7 | 7.8 | 2.1 |
| Asymmetric, smooth | 8,900 | — | — | — |
| Asymmetric, riblets | 8,900 | — | — | — |
| Symmetric, smooth | 33,150 | 5.7 | 7.8 | 2.1 |
| Symmetric, riblets | 33,150 | 5.5 | 8.4 | 2.9 |
| Asymmetric, smooth | 33,150 | — | — | — |
| Asymmetric, riblets | 33,150 | 8.8 | 9.5 | 0.7 |
| Symmetric, smooth | 66,260 | 5.8 | 7.9 | 2.1 |
| Symmetric, riblets | 66,260 | 5.3 | 9.0 | 3.7 |
| Asymmetric, smooth | 66,260 | — | — | — |
| Asymmetric, riblets | 66,260 | 8.7 | 9.7 | 1.0 |

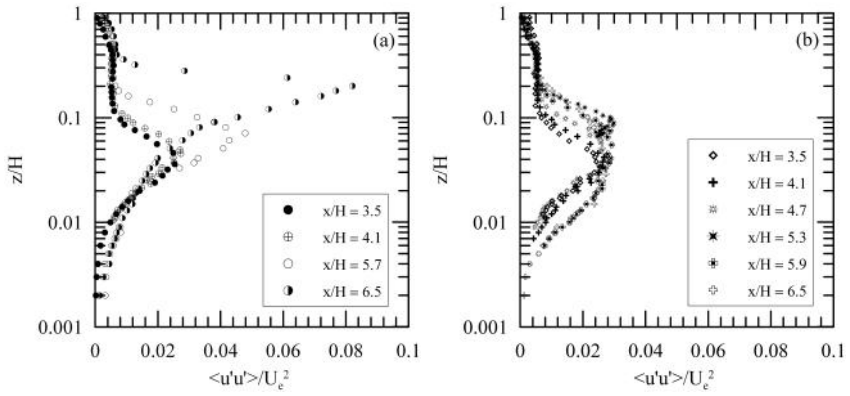


**Figure 9.** Longitudinal turbulent shear stress profiles: (a) symmetric surface, (b) asymmetric surface.

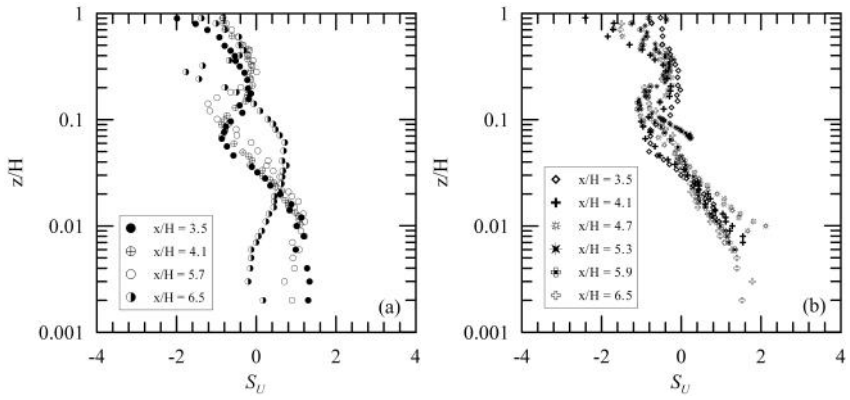


**Figure 10.** Skewness: (a) symmetric surface, (b) asymmetric surface.

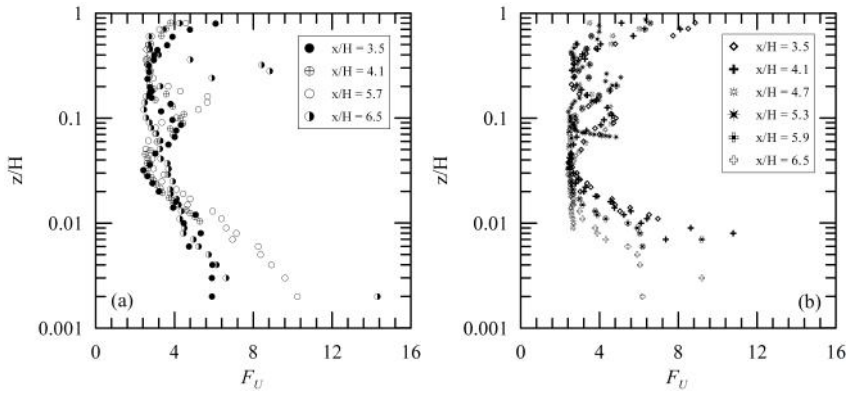


**Figure 11.** Flatness: (a) symmetric surface, (b) asymmetric surface.

Brazilian National Research Council (CNPq) for the award of a Research Fellowship (Grant No 303982/2009-8). The work was financially supported by CNPq through Grants No 473588/2009-9 and by the Rio de Janeiro Research Foundation (FAPERJ) through Grant E-26/170.005/2008.

## References

[1] Becky, L. W., Winn, J. P. & Fish, F. E. 2006 Morphological specialization of Baleen whales associated with hydrodynamic performance and ecological niche. *J. Morphology* **267**, 1284–1294.

[2] Fish, F. E. 1993 Influence of hydrodynamic design and propulsive mode on mammalian swimming energetics. *Aust. J. Zoo.* **42**, 79–101.

[3] Fish, F. E. & Lauder, G. V. 2006 Passive and active flow control by swimming fishes and mammals. *Annu. Rev. Fluid Mech.* **38** 193-224.

[4] Frohnapfel, B., Jovanovic, J. & Delgado, A. 2007 Experimental investigations of turbulent drag reduction by surface-embedded grooves. *J. Fluid Mech.* **590** 107–116.

[5] Gad-el-Hak, M. & Bandyopadhyay, P. R. 1994 Reynolds number effects in wall-bounded turbulent flows. *Appl. Mech. Rev.* **47** 307-365.

[6] Gad-el-Hak, M. 2000 *Flow Control: Passive, Active and Reactive Flow Management.* 448 pp. Cambridge University Press.

[7] Karniadakis, G. E. & Choi, K. S. 2003 Mechanisms on transverse motions in turbulent flows. *Annu. Rev. Fluid Mech.* **35** 45-62.

[8] Loureiro, J. B. R., Pinho, F. T. & Silva Freire A. P. 2007 Near wall characterization of the flow over a two-dimensional steep smooth hill. *Exp. Fluids* **42** 441-457.

[9] Lu, S. S. & Willmarth, W. W. 1973 Measurements of the structure of the Reynolds stress in a turbulent boundary layer. *J. Fluid Mech.* **60** 481-511.

[10] Orlandi, P., Leonardi, S. & Antonia, R. A. 2006 Turbulent channel flow with either transverse or longitudinal roughness elements on one wall. *J. Fluid Mech.* **561** 279-305.

[11] Skote, M. & Hennigson, D. S. 2002 Direct numerical simulation of a separated turbulent boundary layer. *J. Fluid Mech.* **471** 107–136.